Measurement of the W-pair cross-section and of the W mass in e^+e^- interactions at 172 GeV

P. Abreu, W. Adam, T. Adye, P. Adzic, I. Ajinenko, G D. Alekseev, R. Alemany, P P. Allport, S. Almehed, U. Amaldi, et al.

EUROPEAN ORGANIZATION FOR NUCLEAR RESEARCH

CERN–PPE/97–160

16 December 1997

Measurement of the W-pair cross-section and of the W mass in e^+e^- interactions at 172 GeV

DELPHI Collaboration

Abstract

From a data sample of 9.98 pb^{-1} integrated luminosity, collected by DELPHI at a centre-of-mass energy of 172 GeV, 118 events were selected as W-pair candidates. From these, the branching fraction $Br(W \to q\bar{q})$ was measured to be $0.660^{+0.036}_{-0.037}(\text{stat.}) \pm 0.009(\text{syst.})$ and the cross-section for the doubly resonant process $e^+e^- \to W^+W^-$ to be $11.58^{+1.44}_{-1.35}(\text{stat.}) \pm 0.32(\text{syst.})$ pb. The mass of the W boson, obtained from direct reconstruction of the invariant mass of the fermion pairs in the decays $WW \to \ell\nu q\bar{q}$ and $WW \to q\bar{q}q\bar{q}$, was determined to be $m_W = 80.22 \pm 0.41(\text{stat.}) \pm 0.04(\text{syst.}) \pm 0.05(\text{int.}) \pm 0.03(\text{LEP})$ GeV/c^2, where "int." denotes the uncertainty from interconnection effects like colour reconnection and Bose-Einstein interference. Combined with the W mass obtained from the cross-sections measured by DELPHI at threshold, a value of $m_W = 80.33 \pm 0.30(\text{stat.}) \pm 0.05(syst.) \pm 0.03(\text{int.}) \pm 0.03(\text{LEP})$ GeV/c^2 was found.

(Submitted to E. Phys. J. C)

P.Abreu[21], W.Adam[49], T.Adye[36], P.Adzic[11], I.Ajinenko[41], G.D.Alekseev[16], R.Alemany[48], P.P.Allport[22], S.Almehed[24], U.Amaldi[9], S.Amato[46], P.Andersson[43], A.Andreazza[9], P.Antilogus[25], W-D.Apel[17], Y.Arnoud[14], B.Åsman[43], J-E.Augustin[25], A.Augustinus[9], P.Baillon[9], P.Bambade[19], F.Barao[21], G.Barbiellini[45], R.Barbier[25], D.Y.Bardin[16], G.Barker[9], A.Baroncelli[39], O.Barring[24], M.J.Bates[36], M.Battaglia[15], M.Baubillier[23], K-H.Becks[51], M.Begalli[6], P.Beilliere[8], Yu.Belokopytov[9,52], K.Belous[41], A.C.Benvenuti[5], C.Berat[14], M.Berggren[25], D.Bertini[25], D.Bertrand[2], M.Besancon[38], F.Bianchi[44], M.Bigi[44], M.S.Bilenky[16], P.Billoir[23], M-A.Bizouard[19], D.Bloch[10], M.Blume[51], M.Bonesini[27], W.Bonivento[27], M.Boonekamp[38], P.S.L.Booth[22], A.W.Borgland[4], G.Borisov[38], C.Bosio[39], O.Botner[47], E.Boudinov[30], B.Bouquet[19], C.Bourdarios[19], T.J.V.Bowcock[22], I.Bozovic[11], M.Bozzo[13], P.Branchini[39], K.D.Brand[35], T.Brenke[51], R.A.Brenner[47], R.Brown[9], P.Bruckman[35], J-M.Brunet[8], L.Bugge[32], T.Buran[32], T.Burgsmueller[51], P.Buschmann[51], S.Cabrera[48], M.Caccia[27], M.Calvi[27], A.J.Camacho Rozas[40], T.Camporesi[9], V.Canale[37], M.Canepa[13], F.Carena[9], L.Carroll[22], C.Caso[13], M.V.Castillo Gimenez[48], A.Cattai[9], F.R.Cavallo[5], Ch.Cerruti[10], V.Chabaud[9], N.Chalanda[41], Ph.Charpentier[9], L.Chaussard[25], P.Checchia[35], G.A.Chelkov[16], M.Chen[2], R.Chierici[44], P.Chliapnikov[41], P.Chochula[7], V.Chorowicz[25], J.Chudoba[29], V.Cindro[42], P.Collins[9], M.Colomer[48], R.Contri[13], E.Cortina[48], G.Cosme[19], F.Cossutti[9], J-H.Cowell[22], H.B.Crawley[1], D.Crennell[36], G.Crosetti[13], J.Cuevas Maestro[33], S.Czellar[15], B.Dalmagne[19], G.Damgaard[28], P.D.Dauncey[36], M.Davenport[9], W.Da Silva[23], A.Deghorain[2], G.Della Ricca[45], P.Delpierre[26], N.Demaria[9], A.De Angelis[9], W.De Boer[17], S.De Brabandere[2], C.De Clercq[2], C.De La Vaissiere[23], B.De Lotto[45], A.De Min[35], L.De Paula[46], H.Dijkstra[9], L.Di Ciaccio[37], A.Di Diodato[37], A.Djannati[8], J.Dolbeau[8], K.Doroba[50], M.Dracos[10], J.Drees[51], K.-A.Drees[51], M.Dris[31], A.Duperrin[25], J-D.Durand[25,9], D.Edsall[1], R.Ehret[17], G.Eigen[4], T.Ekelof[47], G.Ekspong[43], M.Ellert[47], M.Elsing[9], J-P.Engel[10], B.Erzen[42], M.Espirito Santo[21], E.Falk[24], G.Fanourakis[11], D.Fassouliotis[45], J.Fayot[23], M.Feindt[17], P.Ferrari[27], A.Ferrer[48], S.Fichet[23], A.Firestone[1], P.-A.Fischer[9], U.Flagmeyer[51], H.Foeth[9], E.Fokitis[31], F.Fontanelli[13], F.Formenti[9], B.Franek[36], A.G.Frodesen[4], R.Fruhwirth[49], F.Fulda-Quenzer[19], J.Fuster[48], A.Galloni[22], D.Gamba[44], M.Gandelman[46], C.Garcia[48], J.Garcia[40], C.Gaspar[9], M.Gaspar[46], U.Gasparini[35], Ph.Gavillet[9], E.N.Gazis[31], D.Gele[10], J-P.Gerber[10], N.Ghodbane[25], F.Glege[51], R.Gokieli[50], B.Golob[42], P.Goncalves[21], I.Gonzalez Caballero[40], G.Gopal[36], L.Gorn[1,53], M.Gorski[50], Yu.Gouz[41], V.Gracco[13], J.Grahl[1], E.Graziani[39], C.Green[22], A.Grefrath[51], P.Gris[38], G.Grosdidier[19], K.Grzelak[50], M.Gunther[47], J.Guy[36], F.Hahn[9], S.Hahn[51], S.Haider[9], Z.Hajduk[18], A.Hallgren[47], K.Hamacher[51], F.J.Harris[34], V.Hedberg[24], S.Heising[17], R.Henriques[21], J.J.Hernandez[48], P.Herquet[2], H.Herr[9], T.L.Hessing[34], J.-M.Heuser[51], E.Higon[48], S-O.Holmgren[43], P.J.Holt[34], D.Holthuizen[30], S.Hoorelbeke[2], M.Houlden[22], J.Hrubec[49], K.Huet[2], K.Hultqvist[43], J.N.Jackson[22], R.Jacobsson[43], P.Jalocha[9], R.Janik[7], Ch.Jarlskog[24], G.Jarlskog[24], P.Jarry[38], B.Jean-Marie[19], E.K.Johansson[43], L.Jonsson[24], P.Jonsson[24], C.Joram[9], P.Juillot[10], F.Kapusta[23], K.Karafasoulis[11], S.Katsanevas[25], E.C.Katsoufis[31], R.Keranen[4], B.A.Khomenko[16], N.N.Khovanski[16], B.King[22], N.J.Kjaer[30], O.Klapp[51], H.Klein[9], P.Kluit[30], D.Knoblauch[17], P.Kokkinias[11], M.Koratzinos[9], K.Korcyl[18], C.Kourkoumelis[3], O.Kouznetsov[16], M.Krammer[49], C.Kreuter[9], I.Kronkvist[24], Z.Krumstein[16], P.Kubinec[7], W.Kucewicz[18], K.Kurvinen[15], C.Lacasta[9], J.W.Lamsa[1], L.Lanceri[45], D.W.Lane[1], P.Langefeld[51], V.Lapin[41], J-P.Laugier[38], R.Lauhakangas[15], G.Leder[49], F.Ledroit[14], V.Lefebure[2], C.K.Legan[1], A.Leisos[11], R.Leitner[29], J.Lemonne[2], G.Lenzen[51], V.Lepeltier[19], T.Lesiak[18], M.Lethuillier[38], J.Libby[34], D.Liko[9], A.Lipniacka[43], I.Lippi[35], B.Loerstad[24], J.G.Loken[34], J.H.Lopes[46], J.M.Lopez[40], D.Loukas[11], P.Lutz[38], L.Lyons[34], J.MacNaughton[49], J.R.Mahon[6], A.Maio[21], A.Malek[51], T.G.M.Malmgren[43], V.Malychev[16], F.Mandl[49], J.Marco[40], R.Marco[40], B.Marechal[46], M.Margoni[35], J-C.Marin[9], C.Mariotti[9], A.Markou[11], C.Martinez-Rivero[33], F.Martinez-Vidal[48], S.Marti i Garcia[22], F.Matorras[40], C.Matteuzzi[27], G.Matthiae[37], F.Mazzucato[35], M.Mazzucato[35], M.Mc Cubbin[22], R.Mc Kay[1], R.Mc Nulty[9], G.Mc Pherson[22], J.Medbo[47], C.Meroni[27], W.T.Meyer[1], A.Miagkov[41], M.Michelotto[35], E.Migliore[44], L.Mirabito[25], W.A.Mitaroff[49], U.Mjoernmark[24], T.Moa[43], R.Moeller[28], K.Moenig[9], M.R.Monge[13], X.Moreau[23], P.Morettini[13], K.Muenich[51], M.Mulders[30], L.M.Mundim[6], W.J.Murray[36], B.Muryn[14,18], G.Myatt[34], T.Myklebust[32], F.Naraghi[14], F.L.Navarria[5], S.Navas[48], K.Nawrocki[50], P.Negri[27], S.Nemecek[12], N.Neufeld[9], W.Neumann[51], N.Neumeister[49], R.Nicolaidou[14], B.S.Nielsen[28], M.Nieuwenhuizen[30], V.Nikolaenko[10], M.Nikolenko[10,16], P.Niss[43], A.Nomerotski[35], A.Normand[22], A.Nygren[24], W.Oberschulte-Beckmann[17], V.Obraztsov[41], A.G.Olshevski[16], A.Onofre[21], R.Orava[15], G.Orazi[10], S.Ortuno[48], K.Osterberg[15], A.Ouraou[38], P.Paganini[19], M.Paganoni[27], S.Paiano[5], R.Pain[23], R.Paiva[21], H.Palka[18], Th.D.Papadopoulou[31], K.Papageorgiou[11], L.Pape[9], C.Parkes[34], F.Parodi[13], U.Parzefall[22], A.Passeri[39], M.Pegoraro[35], L.Peralta[21], H.Pernegger[49], M.Pernicka[49], A.Perrotta[5], C.Petridou[45], A.Petrolini[13], H.T.Phillips[36], G.Piana[13], F.Pierre[38], M.Pimenta[21], E.Piotto[35], T.Podobnik[34], O.Podobrin[9], M.E.Pol[6], G.Polok[18], P.Poropat[45], V.Pozdniakov[16], P.Privitera[37], N.Pukhaeva[16], A.Pullia[27], D.Radojicic[34], S.Ragazzi[27], H.Rahmani[31], J.Rames[12], P.N.Ratoff[20], A.L.Read[32], P.Rebecchi[9], N.G.Redaelli[27], M.Regler[49], D.Reid[9], R.Reinhardt[51], P.B.Renton[34], L.K.Resvanis[3], F.Richard[19], J.Ridky[12], G.Rinaudo[44], O.Rohne[32], A.Romero[44], P.Ronchese[35], E.I.Rosenberg[1], P.Rosinsky[7], P.Roudeau[19], T.Rovelli[5], V.Ruhlmann-Kleider[38], A.Ruiz[40], H.Saarikko[15], Y.Sacquin[38], A.Sadovsky[16], G.Sajot[14], J.Salt[48], D.Sampsonidis[11], M.Sannino[13], H.Schneider[17], U.Schwickerath[17], M.A.E.Schyns[51], F.Scuri[45], P.Seager[20], Y.Sedykh[16], A.M.Segar[34], R.Sekulin[36], R.C.Shellard[6], A.Sheridan[22], R.Silvestre[38], F.Simonetto[35], A.N.Sisakian[16], T.B.Skaali[32], G.Smadja[25], N.Smirnov[41], O.Smirnova[24], G.R.Smith[36], O.Solovianov[41], A.Sopczak[17], R.Sosnowski[50], D.Souza-Santos[6], T.Spassov[21], E.Spiriti[39], P.Sponholz[51], S.Squarcia[13], D.Stampfer[9], C.Stanescu[39], S.Stanic[42], S.Stapnes[32], I.Stavitski[35], K.Stevenson[34], A.Stocchi[19], J.Strauss[49], R.Strub[10], B.Stugu[4], M.Szczekowski[50], M.Szeptycka[50],

T.Tabarelli[27], F.Tegenfeldt[47], F.Terranova[27], J.Thomas[34], A.Tilquin[26], J.Timmermans[30], L.G.Tkatchev[16], T.Todorov[10], S.Todorova[10], D.Z.Toet[30], A.Tomaradze[2], B.Tome[21], A.Tonazzo[27], L.Tortora[39], G.Transtromer[24], D.Treille[9], G.Tristram[8], A.Trombini[19], C.Troncon[27], A.Tsirou[9], M-L.Turluer[38], I.A.Tyapkin[16], M.Tyndel[36], S.Tzamarias[11], B.Ueberschaer[51], O.Ullaland[9], V.Uvarov[41], G.Valenti[5], E.Vallazza[45], C.Vander Velde[2], G.W.Van Apeldoorn[30], P.Van Dam[30], W.K.Van Doninck[2], J.Van Eldik[30], A.Van Lysebetten[2], I.Van Vulpen[30], N.Vassilopoulos[34], G.Vegni[27], L.Ventura[35], W.Venus[36], F.Verbeure[2], M.Verlato[35], L.S.Vertogradov[16], V.Verzi[37], D.Vilanova[38], P.Vincent[23], N.Vishnevsky[41], L.Vitale[45], E.Vlasov[41], A.S.Vodopyanov[16], V.Vrba[12], H.Wahlen[51], C.Walck[43], C.Weiser[17], A.M.Wetherell[9], D.Wicke[51], J.H.Wickens[2], G.R.Wilkinson[9], W.S.C.Williams[34], M.Winter[10], M.Witek[18], T.Wlodek[19], G.Wolf[9], J.Yi[1], O.Yushchenko[41], A.Zaitsev[41], A.Zalewska[18], P.Zalewski[50], D.Zavrtanik[42], E.Zevgolatakos[11], N.I.Zimin[16], G.C.Zucchelli[43], G.Zumerle[35]

[1] Department of Physics and Astronomy, Iowa State University, Ames IA 50011-3160, USA
[2] Physics Department, Univ. Instelling Antwerpen, Universiteitsplein 1, BE-2610 Wilrijk, Belgium
and IIHE, ULB-VUB, Pleinlaan 2, BE-1050 Brussels, Belgium
and Faculté des Sciences, Univ. de l'Etat Mons, Av. Maistriau 19, BE-7000 Mons, Belgium
[3] Physics Laboratory, University of Athens, Solonos Str. 104, GR-10680 Athens, Greece
[4] Department of Physics, University of Bergen, Allégaten 55, NO-5007 Bergen, Norway
[5] Dipartimento di Fisica, Università di Bologna and INFN, Via Irnerio 46, IT-40126 Bologna, Italy
[6] Centro Brasileiro de Pesquisas Físicas, rua Xavier Sigaud 150, BR-22290 Rio de Janeiro, Brazil
and Depto. de Física, Pont. Univ. Católica, C.P. 38071 BR-22453 Rio de Janeiro, Brazil
and Inst. de Física, Univ. Estadual do Rio de Janeiro, rua São Francisco Xavier 524, Rio de Janeiro, Brazil
[7] Comenius University, Faculty of Mathematics and Physics, Mlynska Dolina, SK-84215 Bratislava, Slovakia
[8] Collège de France, Lab. de Physique Corpusculaire, IN2P3-CNRS, FR-75231 Paris Cedex 05, France
[9] CERN, CH-1211 Geneva 23, Switzerland
[10] Institut de Recherches Subatomiques, IN2P3 - CNRS/ULP - BP20, FR-67037 Strasbourg Cedex, France
[11] Institute of Nuclear Physics, N.C.S.R. Demokritos, P.O. Box 60228, GR-15310 Athens, Greece
[12] FZU, Inst. of Phys. of the C.A.S. High Energy Physics Division, Na Slovance 2, CZ-180 40, Praha 8, Czech Republic
[13] Dipartimento di Fisica, Università di Genova and INFN, Via Dodecaneso 33, IT-16146 Genova, Italy
[14] Institut des Sciences Nucléaires, IN2P3-CNRS, Université de Grenoble 1, FR-38026 Grenoble Cedex, France
[15] Helsinki Institute of Physics, HIP, P.O. Box 9, FI-00014 Helsinki, Finland
[16] Joint Institute for Nuclear Research, Dubna, Head Post Office, P.O. Box 79, RU-101 000 Moscow, Russian Federation
[17] Institut für Experimentelle Kernphysik, Universität Karlsruhe, Postfach 6980, DE-76128 Karlsruhe, Germany
[18] Institute of Nuclear Physics and University of Mining and Metalurgy, Ul. Kawiory 26a, PL-30055 Krakow, Poland
[19] Université de Paris-Sud, Lab. de l'Accélérateur Linéaire, IN2P3-CNRS, Bât. 200, FR-91405 Orsay Cedex, France
[20] School of Physics and Chemistry, University of Lancaster, Lancaster LA1 4YB, UK
[21] LIP, IST, FCUL - Av. Elias Garcia, 14-1^{o}, PT-1000 Lisboa Codex, Portugal
[22] Department of Physics, University of Liverpool, P.O. Box 147, Liverpool L69 3BX, UK
[23] LPNHE, IN2P3-CNRS, Univ. Paris VI et VII, Tour 33 (RdC), 4 place Jussieu, FR-75252 Paris Cedex 05, France
[24] Department of Physics, University of Lund, Sölvegatan 14, SE-223 63 Lund, Sweden
[25] Université Claude Bernard de Lyon, IPNL, IN2P3-CNRS, FR-69622 Villeurbanne Cedex, France
[26] Univ. d'Aix - Marseille II - CPP, IN2P3-CNRS, FR-13288 Marseille Cedex 09, France
[27] Dipartimento di Fisica, Università di Milano and INFN, Via Celoria 16, IT-20133 Milan, Italy
[28] Niels Bohr Institute, Blegdamsvej 17, DK-2100 Copenhagen Ø, Denmark
[29] NC, Nuclear Centre of MFF, Charles University, Areal MFF, V Holesovickach 2, CZ-180 00, Praha 8, Czech Republic
[30] NIKHEF, Postbus 41882, NL-1009 DB Amsterdam, The Netherlands
[31] National Technical University, Physics Department, Zografou Campus, GR-15773 Athens, Greece
[32] Physics Department, University of Oslo, Blindern, NO-1000 Oslo 3, Norway
[33] Dpto. Fisica, Univ. Oviedo, Avda. Calvo Sotelo s/n, ES-33007 Oviedo, Spain, (CICYT-AEN96-1681)
[34] Department of Physics, University of Oxford, Keble Road, Oxford OX1 3RH, UK
[35] Dipartimento di Fisica, Università di Padova and INFN, Via Marzolo 8, IT-35131 Padua, Italy
[36] Rutherford Appleton Laboratory, Chilton, Didcot OX11 OQX, UK
[37] Dipartimento di Fisica, Università di Roma II and INFN, Tor Vergata, IT-00173 Rome, Italy
[38] DAPNIA/Service de Physique des Particules, CEA-Saclay, FR-91191 Gif-sur-Yvette Cedex, France
[39] Istituto Superiore di Sanità, Ist. Naz. di Fisica Nucl. (INFN), Viale Regina Elena 299, IT-00161 Rome, Italy
[40] Instituto de Fisica de Cantabria (CSIC-UC), Avda. los Castros s/n, ES-39006 Santander, Spain,
(CICYT-AEN96-1681)
[41] Inst. for High Energy Physics, Serpukov P.O. Box 35, Protvino, (Moscow Region), Russian Federation
[42] J. Stefan Institute, Jamova 39, SI-1000 Ljubljana, Slovenia and Department of Astroparticle Physics, School of
Environmental Sciences, Kostanjeviska 16a, Nova Gorica, SI-5000 Slovenia,
and Department of Physics, University of Ljubljana, SI-1000 Ljubljana, Slovenia
[43] Fysikum, Stockholm University, Box 6730, SE-113 85 Stockholm, Sweden
[44] Dipartimento di Fisica Sperimentale, Università di Torino and INFN, Via P. Giuria 1, IT-10125 Turin, Italy
[45] Dipartimento di Fisica, Università di Trieste and INFN, Via A. Valerio 2, IT-34127 Trieste, Italy
and Istituto di Fisica, Università di Udine, IT-33100 Udine, Italy
[46] Univ. Federal do Rio de Janeiro, C.P. 68528 Cidade Univ., Ilha do Fundão BR-21945-970 Rio de Janeiro, Brazil
[47] Department of Radiation Sciences, University of Uppsala, P.O. Box 535, SE-751 21 Uppsala, Sweden
[48] IFIC, Valencia-CSIC, and D.F.A.M.N., U. de Valencia, Avda. Dr. Moliner 50, ES-46100 Burjassot (Valencia), Spain
[49] Institut für Hochenergiephysik, Österr. Akad. d. Wissensch., Nikolsdorfergasse 18, AT-1050 Vienna, Austria
[50] Inst. Nuclear Studies and University of Warsaw, Ul. Hoza 69, PL-00681 Warsaw, Poland
[51] Fachbereich Physik, University of Wuppertal, Postfach 100 127, DE-42097 Wuppertal, Germany
[52] On leave of absence from IHEP Serpukhov
[53] Now at University of Florida

1 Introduction

In the autumn of 1996, LEP provided e^+e^- collisions at a centre-of-mass energy, $E_{\rm cms}$, of 170.3 and 172.3 GeV. DELPHI collected data corresponding to a total integrated luminosity of 9.98 pb^{-1} at a luminosity weighted average energy of 172.14 GeV. At these energies the ratio of the expected cross-section for W-pair production to the background is about a factor four higher than at the nominal threshold. The sensitivity of the W-pair production cross-section to the W mass is however much reduced, compared to the cross-section at threshold. Instead, at these higher energies, the measurement of the W mass can be made by direct reconstruction of the invariant mass of the fermion pairs from each W decay, using constrained fitting techniques.

This paper is organized as follows. In Section 2, the DELPHI detector setup, the event trigger, the luminosity measurement, and the event generators are briefly reviewed. The track selection and lepton identification are described in Section 3. Section 4 presents the event selection and the computation of cross-sections for the different decay channels, and the branching fraction $\mathrm{Br}(\mathrm{W} \to \mathrm{q\bar{q}})$ and the total cross-section are derived. The measurements of the W mass from direct reconstruction are given in Section 5. Finally, a combined value for $m_{\rm W}$ from direct reconstruction and from the WW production cross-sections measured at centre-of-mass energies of 161 GeV [1] and 172 GeV is given in Section 6.

2 Apparatus, Trigger, Luminosity and Simulations

Detailed descriptions of the DELPHI apparatus and its performance can be found in [2,3]. In 1996 the cylindrical 3-layer vertex detector was lengthened and complemented with additional silicon detectors covering the endcap region.

The event trigger is described in [2,3]. From trigger efficiencies measured for single charged particles with redundant trigger combinations, the efficiency for two charged particles (which is the worst case for all events of interest in the present analysis) was found to exceed 99%.

The luminosity was measured using the Small Angle Tile Calorimeter (STIC). It consists of two lead/scintillator sampling calorimeters, located at $\pm$ 220 cm from the interaction point, providing full coverage of the region between 29 and 185 mrad with respect to the beam axis. A detailed description of this detector can be found in [4]. Events corresponding to Bhabha scattering were selected by requiring a coincidence of two electromagnetic showers coplanar with the beam axis, each with energy larger than 65% of the beam energy. In order to minimize the sensitivity to the position of the interaction point, asymmetric cuts were imposed on the reconstructed radii of the two showers.

The response of the detector to various physics processes was modelled using the full simulation program DELSIM [3], which incorporates the resolution, granularity, and efficiency of the detector components.

The calculation of the accepted Bhabha cross-section was based on the event generator BHLUMI 4.03 [5], which has a theoretical accuracy of 0.25% at LEP2 energies. The generated events were passed through a full simulation of the detector, and analysed in the same way as the real data. The total experimental systematic error on the luminosity amounts to 0.5%, with the main contribution arising from the uncertainty in the radial cuts. For the data sample used, the integrated luminosity was found to be $9.98 \pm 0.05(\mathrm{stat.}) \pm 0.06(\mathrm{syst.})$ pb^{-1}.

In order to study efficiencies, background contributions, and mass resolutions, the event generator PYTHIA 5.7 [6] was chosen with the fragmentation tuned to the DELPHI data measured at LEP1 [7]; the generated events were passed through the full DELPHI simulation and analysis programs. The WW signal events were generated with $m_{\mathrm{W}} = 80.35$ GeV/c^2 and an s-dependent width of $\Gamma_{\mathrm{W}} = 2.07$ GeV/c^2. For the W direct mass reconstruction event samples were generated with varying values of m_{W}. The backgrounds from $\mathrm{e^+e^-} \to \mathrm{Z}(\gamma)$, $\mathrm{e^+e^-} \to \mathrm{ZZ}$, $\mathrm{e^+e^-} \to \mathrm{Ze^+e^-}$, and single W production were also generated with PYTHIA, while the background from two photon processes was found to be negligible except for the fully leptonic decay modes. Systematic checks were performed using other generators as described in the relevant sections.

3 Track Selection and Lepton Identification

Charged particles were selected if they fulfilled the following criteria:

- polar angle with respect to the electron beam direction between 10° and 170°;
- momentum greater than 0.4 GeV/c;
- good track quality, assessed as follows:
  - track length greater than 15 cm;
  - impact parameters with respect to the nominal interaction point less than 4 cm transverse and less than 4 cm/$\sin\theta$ longitudinal where θ is the polar angle with respect to the electron beam direction;
  - estimated relative error on momentum measurement less than 100%.

For neutral particles the following selection criteria were applied :

- energy of the shower greater than 0.5 GeV;
- additional requirements on shower quality, assessed as follows:
  - showers in the STIC calorimeter with deposits in more than one cell;
  - showers in the hadron calorimeter with energy uncertainties below 100%.

Electron identification was performed in the polar angle range between 20° and 160° by looking for charged particles with a characteristic energy deposition in the central and forward/backward electromagnetic calorimeters. The energy was required to be within 20% of the measured track momentum or to exceed 20 GeV. For this polar angle range the identification efficiency for high energy electrons was determined from simulation to be $(77 \pm 2)\%$, in good agreement with efficiencies determined using Bhabha events measured in the detector.

Tracks were identified as due to muons if they had at least one associated hit in the muon chambers, or an energy deposition in the hadron calorimeter consistent with a minimum ionizing particle. Muon identification was performed in the polar angle range between 10° and 170°. Within this acceptance, the identification efficiency was determined from simulation to be $(92 \pm 1)\%$. Good agreement was found between data and simulation for high momentum muons in $\mathrm{Z} \to \mu^+\mu^-$ decays, and for low momentum pairs produced in $\gamma\gamma$ reactions.

4 Event Selection and Cross-Sections

The analysis described here is similar to the one used for the measurement of the threshold cross-section at 161.3 GeV [1]. At 172 GeV, the ratio of the signal cross-section

to the cross-section of Z/γ events is about four times larger than at threshold. This allows some of the selection criteria to be relaxed and improves the efficiency of the selections. Other selection criteria are rescaled in accordance with the increase in total energy.

The cross-sections determined in this analysis are defined to correspond to W pair production through the three doubly resonant tree-level diagrams ("CC03 diagrams" [8]) involving s-channel γ and Z exchange and t-channel ν exchange. The selection efficiencies given in this section are also defined with respect to these diagrams only. Depending on the decay mode of each W, fully hadronic, mixed hadronic-leptonic ("semileptonic"), or fully leptonic final states are obtained. The Standard Model branching fractions are 45.9%, 43.7% and 10.4% respectively. In addition to their production via the CC03 diagrams, the four-fermion final states corresponding to these decay modes may be produced via other diagrams involving either zero, one, or two massive vector bosons. The effects of the interference between the CC03 diagrams and the additional diagrams have been taking into account using correction factors [1], which were applied such that the cross-sections given below can be compared to theoretical estimates of the CC03 cross-sections. The numerical values of these correction factors at a centre-of-mass energy of 172 GeV are given in Table 1. The uncertainties are estimated to be about 1.5% and are taken into account in the systematic uncertainties on the cross-sections given below. The correction factors are consistent with unity within errors.

WW decay mode	C_{CC03}
$\mathrm{q\bar{q}q\bar{q}}$	0.980
$\mathrm{e}\nu\mathrm{q\bar{q}}$	1.019
$\mu(\tau)\nu\mathrm{q\bar{q}}$	0.996
$\ell\nu\ell\nu$	0.980

Table 1: Correction factors C_{CC03} for the decay modes of WW pairs. For $\ell\nu\ell\nu$ the correction factor given is the combined value for all lepton combinations.

4.1 Fully Hadronic Final State

The event selection criteria were optimized in order to ensure that the final state was purely hadronic and in order to reduce the residual background. The background is dominated by electron-positron annihilation into $\mathrm{q\bar{q}}(\gamma)$, with a cross-section about one order of magnitude larger than that for the signal.

For each event, all particles were clustered into jets using the LUCLUS algorithm [9] with $d_{\mathrm{join}} = 6.0$ GeV/c. At least 4 jets were required, with at least four particles in each jet. Events coming from the radiative return to the Z peak were rejected by requiring $\sqrt{s'} > 100$ GeV, where $\sqrt{s'}$ is an estimate of the effective collision energy after initial state radiation [10]. The events in the $\sqrt{s'}$ calculation were forced into 2 jets. Assuming one missing photon in either beam direction, $\sqrt{s'}$ was then derived from the angles of the 2 jets with respect to the electron beam direction.

Events were then forced into a 4-jet configuration, and a kinematically constrained fit performed, imposing energy and momentum conservation. For the separation of WW events and $\mathrm{q\bar{q}}(\gamma)$ events the variable D is used:

$$D = \frac{E_{\mathrm{min}}}{E_{\mathrm{max}}} \cdot \frac{\theta_{\mathrm{min}}}{(E_{\mathrm{max}} - E_{\mathrm{min}})}, \tag{1}$$

where $E_{\rm min}$, $E_{\rm max}$ are the minimum and maximum jet energies and $\theta_{\rm min}$ is the smallest interjet angle after the constrained fit. The variable D was required to exceed 0.004 GeV^{-1}. Figure 1 shows the distribution of this quantity after the other cuts described above.

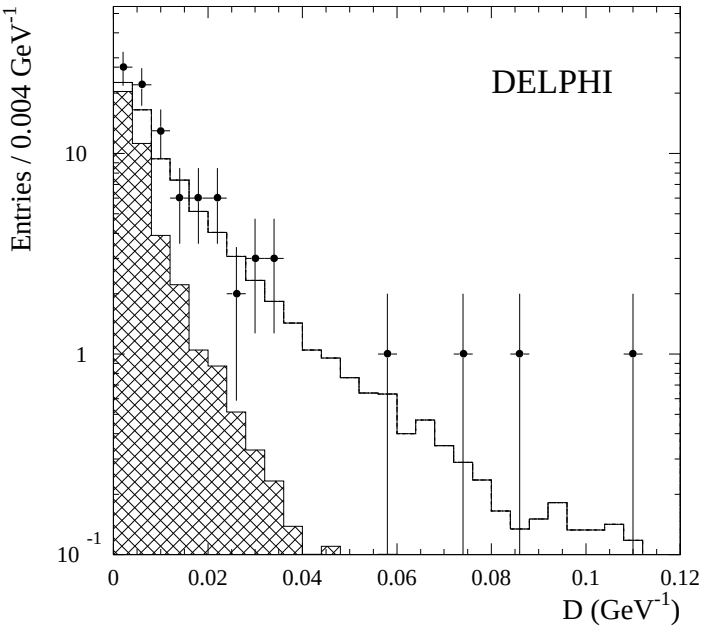

Figure 1: Distribution of the D variable (as defined in the text) for 4-jet events with effective centre-of-mass energy greater than 100 GeV. The data (points with error bars) are compared with simulated $q\bar{q}(\gamma)$ background (cross-hatched areas) and WW signal (white areas) normalized to the fitted cross-section.

The selection efficiency was computed from simulation to be $(82.7 \pm 1.6)\%$. The error includes the systematic uncertainty, which was estimated by varying all selection criteria by at least the value of their experimental resolutions and taking the quadratic sum of all contributions.

A residual background cross-section of 2.14 ± 0.16 pb was estimated, with the dominant contribution coming from e^+e^- annihilation into $q\bar{q}(\gamma)$ events, 1.6% of which survived the WW selection procedure, corresponding to a residual cross-section of 1.96 pb. The other contributions come from the channel $e^+e^- \to ZZ$ (0.11 pb) and the semileptonic final states of $e^+e^- \to W^+W^-$ (0.06 pb), while the background from $e^+e^- \to Ze^+e^-$ is negligible. The systematic uncertainty on the background was estimated from the variation of the selection efficiency for the $q\bar{q}(\gamma)$ background using different generators. Furthermore the accuracy of the simulation was checked on multihadronic events collected at the Z pole. These data were selected with the 172 GeV criteria downscaled in proportion to the collision energy, and good agreement was found with the expected numbers of events.

From the full data sample, 65 events were selected. The cross-section for fully hadronic events was obtained from a binned maximum likelihood fit to the distribution of the variable D for $D > 0.004$, taking into account the expected background in each bin. The result is

$$\sigma_{\mathrm{WW}}^{\mathrm{q\bar{q}q\bar{q}}} = \sigma_{\mathrm{WW}}^{\mathrm{tot}} \times \mathrm{Br}(\mathrm{WW} \to \mathrm{q\bar{q}q\bar{q}}) = 4.74^{+0.95}_{-0.86} \pm 0.18 \text{ pb},$$

where $\mathrm{Br}(\mathrm{WW} \to \mathrm{q\bar{q}q\bar{q}})$ is the probability for the WW pair to give a purely hadronic final state, and the first error is statistical and the second is systematic. The dominant contribution to the systematic error (0.15 pb) comes from the uncertainty on the background. The other components are due to the uncertainties in the efficiency, CC03 factor and luminosity.

4.2 Semileptonic Final States

Events in which one W decays into $\ell\nu$ and the other into quarks are characterized by two hadronic jets, one isolated lepton (coming either from W decay or from the cascade decay $\mathrm{W} \to \tau\nu \to e\nu\nu$ or $\mu\nu\nu$) or a low multiplicity jet due to τ decay, and a missing momentum resulting from the neutrino(s). The major background comes from $\mathrm{q\bar{q}}(\gamma)$ production and from four-fermion final states containing two quarks and two leptons of the same flavour.

The events were required to contain at least 6 charged particles with total energy of at least $0.15\,E_{\mathrm{cms}}$. Events with a detected photon of energy > 30 GeV were rejected. In the case of WW decays into $\mathrm{q\bar{q}}\mu\nu$ and $\mathrm{q\bar{q}}e\nu$ the candidate lepton was required to be the most energetic charged particle in the event, while the τ candidates were selected by looking for an isolated e or μ or a jet of multiplicity ≤ 5 with ≤ 3 charged particles and total momentum > 10 GeV/c.

The muon candidates were required to have momentum > 5 GeV/c, and the isolation angle between the candidate muon and the nearest charged particle with momentum > 1 GeV/c was required to exceed a value set at 8° for muons identified with hits in the muon chambers, at 12° for muons only identified with the hadron calorimeter, and 20° for unidentified muons with less than 5 GeV in the electromagnetic calorimeters.

The momentum of the electron candidate was required to be > 5 GeV/c and the component of the missing momentum transverse to the beam axis, $p^{\mathrm{t}}_{\mathrm{miss}}$, was required to exceed 10 GeV/c. The isolation angle between the electron direction and the nearest charged particle with momentum above 1 GeV/c was required to exceed a value of 5° for electrons with a deposit in the central calorimeter above 20 GeV, 10° for electrons with a deposit in the forward calorimeter above 20 GeV, and 20° otherwise.

In order to increase the efficiency of the selection, cases where the candidate was either not isolated or not identified as a lepton were also treated. The kinematic requirements in these cases were tighter, rejecting events if the angle between the direction of the missing momentum and the beam axis $< 18°$ (30° for identified electrons) or if $\sqrt{s'}$ $> E_{\mathrm{cms}} - 15$ GeV.

The four-fermion background ($\mathrm{q\bar{q}}\ell\ell$) was suppressed by applying an additional selection to the events in which a second lepton of the same flavour and with charge opposite to that of the candidate was found. The event was rejected if the second lepton had a momentum above 5 GeV/c and an isolation angle with respect to all the other particles except the candidate lepton above 15°.

In the selection of $\mathrm{q\bar{q}}\tau\nu$ events with the τ decaying hadronically, the events were only accepted if at least 3 jets were reconstructed using the LUCLUS [9] algorithm with $d_{\mathrm{join}} = 3$ GeV/c, and if the missing energy and the transverse energy both exceeded 40 GeV. Due to the fact that the $\mathrm{q\bar{q}}(\gamma)$ background is concentrated in two regions of $\sqrt{s'}$ (high energy and radiative return to the Z peak), while the signal is more uniformly distributed, the kinematic requirements were tightened in the unfavourable regions (for $\sqrt{s'}$ below 100 GeV or above 150 GeV).

After the selection of the lepton it was required that the effective mass of the remaining particles exceeded 30 GeV/c^2 and that when these particles were forced into two jets using LUCLUS, each jet had a multiplicity of 4 or more and included at least one charged particle.

Figure 2 shows the distribution of the momentum of the candidate leptons. The efficiency for the signal selection (WW $\to$ q$\bar{\text{q}}\ell\nu$) was determined to be (69.4 $\pm$ 1.1)% (90.1, 75.5 and 42.8 for muon, electron and tau events respectively). A correction to the efficiency of -1.0% has been included to account for the difference in track reconstruction efficiency in data and simulated events and the same amount was added in quadrature to the total systematic error. The expected background contribution after the selection was estimated to be (0.526$\pm$0.079) pb. The errors on the signal efficiency and the background include all systematic uncertainties.

From the full data sample corresponding to an integrated luminosity of 9.98 pb^{-1}, a total of 45 events was selected (17 events with a muon, 14 events with an electron and 14 events with a tau). From this and assuming lepton universality the WW cross-section for semileptonic decays was derived to be:

$$\sigma_{\text{WW}}^{\text{q}\bar{\text{q}}\ell\nu} = \sigma_{\text{WW}}^{\text{tot}} \times \text{Br}(\text{WW} \to \text{q}\bar{\text{q}}\ell\nu) = 5.78\ ^{+1.02}_{-0.93}\ \pm\ 0.17\ \text{pb}\ ,$$

where the first error is statistical and the second systematic. The systematic error has contributions from the uncertainties on the efficiency, the background, the CC03 factor and the luminosity.

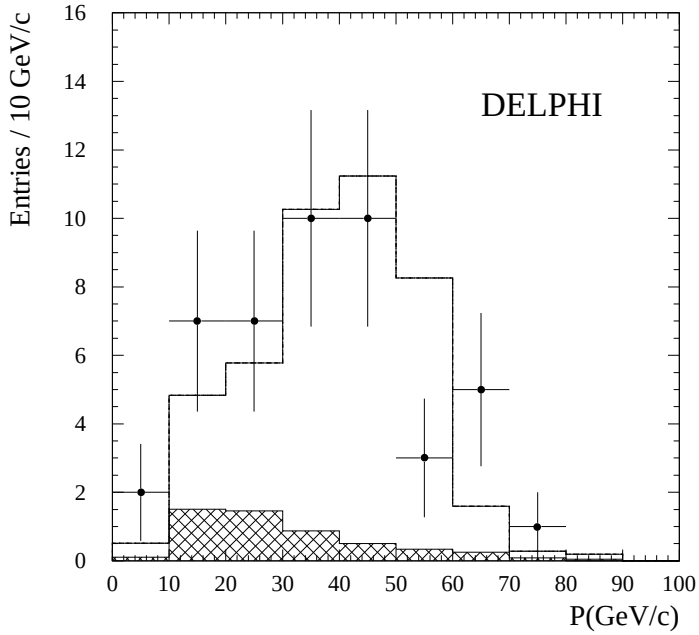

Figure 2: Momentum distribution of the lepton in the semileptonic final states: dots are data and the full line is the SM expectation for the signal (white area) plus the calculated background (cross-hatched area). All cuts were applied except that on the lepton momentum.

4.3 Fully Leptonic Final States

Events in which both W bosons decay into $\ell\nu$ are characterized by two energetic, acollinear and acoplanar leptons of opposite charge, and by large missing energy and momentum. In $W \to e\nu$ and $W \to \mu\nu$ decays, the lepton energy ranges typically between 30 and 60 GeV; $W \to \tau\nu$ decays produce either a single charged particle with a lower momentum, or a narrow jet. The relevant backgrounds are dileptons from $e^+e^- \to Z(\gamma)$, Bhabha scattering and two-photon collisions. In order to select a sample of purely leptonic events, preliminary cuts were applied to all events, followed by the logical 'OR' of three different selections corresponding to different lepton flavour combinations.

For the preselection, a charged particle multiplicity between 2 and 5 was required with the total energy of these particles greater than 30 GeV, and an acollinearity between the two highest momentum particles in the range $10^\circ < \theta_{\rm acol} < 160^\circ$. All particles in the event were then clustered into jets using the LUCLUS algorithm [9] with $d_{\rm join} = 6.5$ GeV/c and only events with two reconstructed jets, containing at least one charged particle each, were retained.

Events from radiative Z production with the ISR photon entering the detector acceptance were greatly reduced by requiring that there be no neutral energy greater than 10 GeV in a cone with an aperture of 10° around the beam direction. To reduce background from $\gamma\gamma \to \ell\ell$ events and radiative dilepton events, two further selection criteria were applied at different values in the extraction of the following three categories of events. The first selection criterion was on the angle $\theta_{\rm miss}$ between the direction of the missing momentum and the beam direction. The second selection was placed on the transverse component of the jet momenta with respect to the 2D-thrust axis ($p_{\rm tr}$), where the 2D-thrust axis was constructed from the projection of the jet momenta onto the plane transverse to the beam direction.

a) e$-\mu$ selection: Events were selected if there was one charged particle with at least 20 GeV of associated electromagnetic energy and one charged particle with momentum greater than 5 GeV/c and identified as a muon as described in Section 3. The value of $|\cos\theta_{\rm miss}|$ was required to be smaller than 0.98 and $p_{\rm tr}$ was required to be greater than 2 GeV/c.

b) $\mu - \tau$ selection: Events were selected if there was one and only one charged particle identified as a muon with hits in the muon chambers and momentum greater than 20 GeV/c. The momentum of the second jet was required to be greater than 10 GeV/c, $|\cos\theta_{\rm miss}|$ was required to be less than 0.94 and $p_{\rm tr}$ to be greater than 1.2 GeV/c.

c) flavour-blind selection: Events were selected if the momentum of the leading jet was between 25 and 70 GeV/c, that of the other jet between 5 and 60 GeV/c and the total momentum in the plane transverse to the beam direction greater than 8 GeV/c. The energy in the electromagnetic calorimeters was required to be less than 110 GeV in total, and less than 70 GeV for a single particle. The value of $|\cos\theta_{\rm miss}|$ was required to be smaller than 0.90 and $p_{\rm tr}$ to be greater than 2 GeV/c.

Figure 3 shows the distribution of $|\cos\theta_{\rm miss}|$ from these three selections. The global efficiency of the selection was estimated to be $(62.6 \pm 2.4)\%$. A correction of -2.0% was applied to the value of the efficiency to account for the difference in the track reconstruction efficiency between data and simulated events and the same amount was added in quadrature to the total systematic error. The residual background from non-W and single-W events is 0.133 ± 0.040 pb.

With the criteria described above 8 events were selected in the full data sample. The cross-section for the purely leptonic final states was calculated to be:

$$\sigma_{\mathrm{WW}}^{\ell\nu\ell\nu} = \sigma_{\mathrm{WW}}^{\mathrm{tot}} \times \mathrm{Br}(\mathrm{WW} \to \ell\nu\ell\nu) = 1.05\ ^{+0.50}_{-0.39}\ \pm 0.09\ \mathrm{pb},$$

where the first error is statistical and the second systematic. The systematic error has contributions from uncertainties in efficiency and background determination, electromagnetic energy calibration, muon identification, evaluation of the CC03 correction factor and the luminosity.

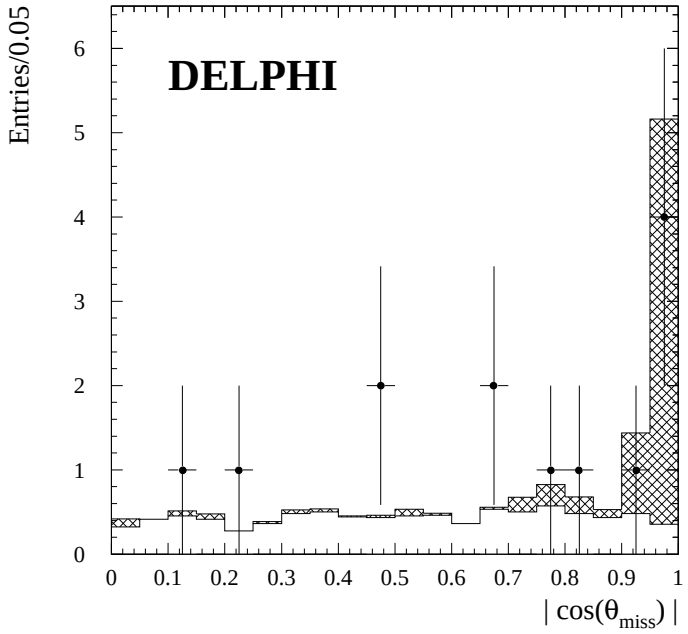

Figure 3: Distribution of $|\cos\theta_{\mathrm{miss}}|$ in the fully leptonic final states: Dots are data and the full line is the SM expectation for the signal (white area) plus the calculated background (cross-hatched area). All cuts were applied except that on $|\cos\theta_{\mathrm{miss}}|$.

4.4 Branching Fractions and Total Cross-section

The total cross-section for WW production and the W branching fractions were obtained from a likelihood fit based on the product of the Poissonian probabilities of finding the observed numbers of events in the fully hadronic, the three semileptonic and the fully leptonic final states. The results for the leptonic branching fractions are given in Table 2 and are consistent with lepton universality. Assuming lepton universality, the fit was repeated including the branching fraction measurement obtained at 161 GeV [1]. The result for the leptonic branching fraction is also given in Table 2, and the derived result for the hadronic branching fraction $\mathrm{Br}(\mathrm{W} \to \mathrm{q\bar{q}})$ is:

$$\mathrm{Br}(\mathrm{W} \to \mathrm{q\bar{q}}) = 0.660^{+0.036}_{-0.037}\ \pm 0.009,$$

where the first error is statistical and the latter is systematic. The systematic error is determined from the estimated errors on efficiency and residual background of the different final states.

$\mathrm{Br}(\mathrm{W} \to \mathrm{e}\nu)$	$0.102^{+0.038}_{-0.032} \pm 0.003$
$\mathrm{Br}(\mathrm{W} \to \mu\nu)$	$0.107^{+0.032}_{-0.027} \pm 0.003$
$\mathrm{Br}(\mathrm{W} \to \tau\nu)$	$0.134^{+0.050}_{-0.048} \pm 0.007$
$\mathrm{Br}(\mathrm{W} \to \ell\nu)$	$0.113^{+0.012}_{-0.012} \pm 0.003$

Table 2: Results for the W leptonic branching fractions. The last row shows the W leptonic branching fraction, measured under the assumption of lepton universality. The first errors are statistical, the latter are systematic.

The branching fraction is in agreement with the Standard Model expectation of 0.677. Combining the results for the cross-sections in the three final states and imposing the SM branching fractions, the total cross-section for WW production is determined to be:

$$\sigma^{\mathrm{tot}}_{\mathrm{WW}} = 11.58\ ^{+1.44}_{-1.35}\ \pm 0.32\ \mathrm{pb},$$

where the first error is statistical and the latter is systematic.

The evolution of the cross-section as a function of the collision energy is shown in Fig. 4 and shows good agreement with the Standard Model prediction determined using GENTLE [11].

5 Direct Reconstruction of the W Boson Mass

Above the threshold for W pair-production the W boson mass can be reconstructed directly from its decay products. A priori, the mass resolution obtained from reconstructing m_{W} from the invariant mass of the $\mathrm{q\bar{q}}$ system is not adequate for a precision measurement due to the jet energy resolution. The mass resolution is improved by imposing constraints from momentum and energy conservation. Although the errors on the two masses reconstructed in an event are large there is a strong negative correlation between them, and the average is well determined with a precision at the level of the W width folded with $\mathcal{O}(1\ \mathrm{GeV}/c^2)$. The constrained fit described below imposed an additional equal mass constraint to obtain only one mass value per fit.

5.1 Event Selection

The event selections used were simplified versions of those described previously for the cross-section measurement. Emphasis was placed on applying only selections that leave the mass measurement unbiased for masses above 25 GeV/c^2.

5.1.1 The Fully Hadronic Channel

The fully hadronic channel has a large background dominated by $\mathrm{q\bar{q}}(\gamma)$ events. In order to retain maximal efficiency, only a loose 4-jet selection was applied. Following the event selection, each event was then treated separately with a signal purity estimated on an event-by-event basis.

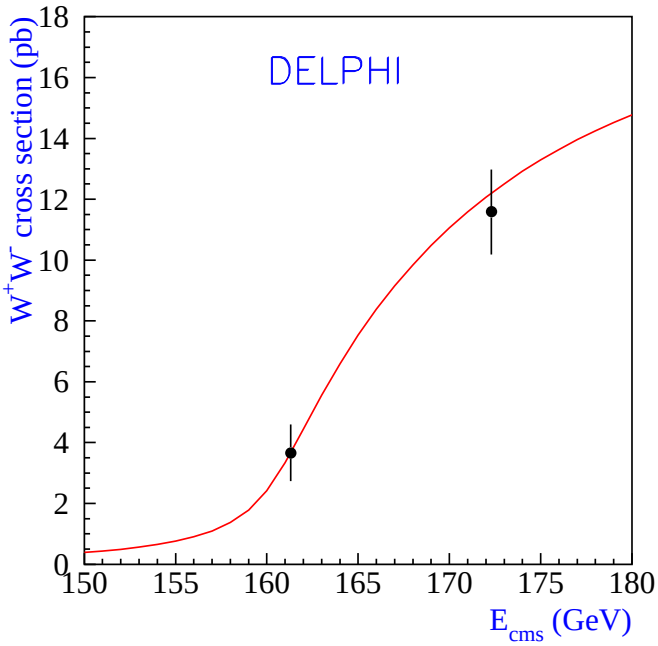

Figure 4: W^+W^- cross-section as a function of centre-of-mass energy. The curve is the Standard Model prediction for $m_W = 80.45$ GeV/c^2.

For each event, all particles were clustered into jets using the DURHAM algorithm [12] with $y_{cut} = 0.001$. The DURHAM algorithm was chosen for its slightly better mass reconstruction performance in simulated events. Only events with at least 4 reconstructed jets were retained. Events with more than 5 reconstructed jets (5% of the signal) were forced into a 5-jet configuration by raising the value of y_{cut}. The events were subsequently treated according to the number of reconstructed jets, 4 or 5. However, in order to reject events from the $q\bar{q}(\gamma)$ final state, a variable D_{pur} was formed by forcing all events to a 4-jet configuration and then calculating the product of the smallest di-jet opening angle and the minimum jet energy:

$$D_{pur} = \theta_{min} \cdot E_{min}. \quad (2)$$

The purity of an event with a given value of D_{pur} was then estimated as the fraction of simulated events which come from the signal, as shown in Fig. 5.

In order to suppress background with significant initial state radiation the following selections were used:

- The total measured energy was required to be above 93 GeV and the total measured energy of neutral particles less than 130 GeV;
- The charged multiplicity had to be at least 19;
- Jets in both 4-jet and 5-jet events were required to have masses above 1 GeV/c^2 and the number of particles in each jet to be at least 4;

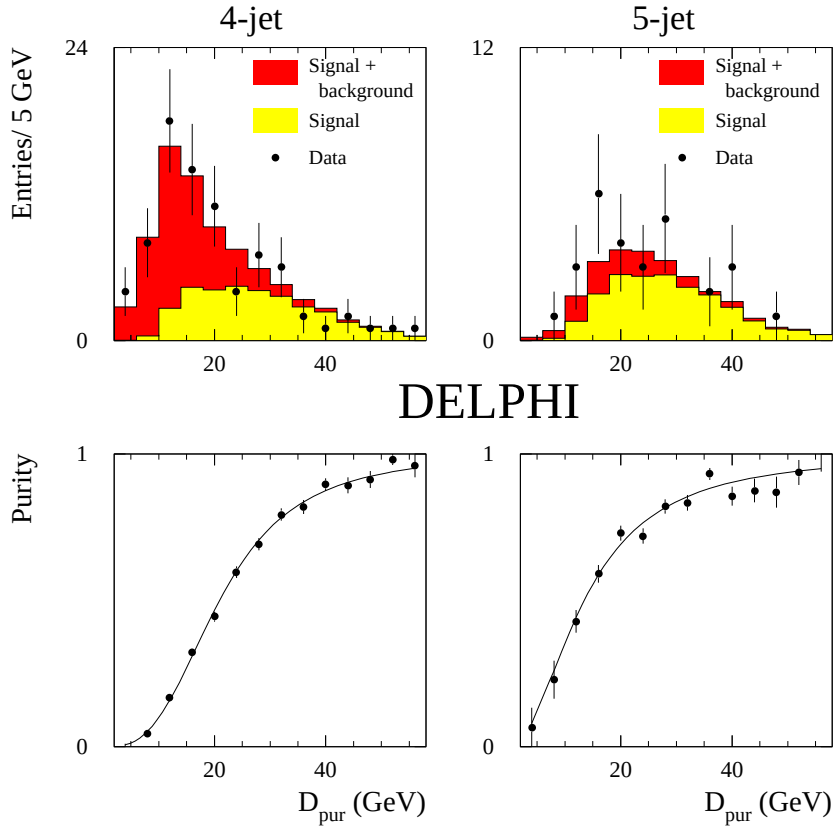

Figure 5: The distribution of $D_{\rm pur}$ for 4-jet and 5-jet events. The lower plots show the purity as a function of $D_{\rm pur}$. The curves correspond to a simple parametrization.

- A 3–C constrained fit (see below) assuming energy and momentum conservation and an undetected photon parallel to the beam direction was required to give an estimate of the photon energy below 25 GeV.

The overall efficiency was found from simulation to be $(89.0 \pm 1.0)\%$ with a residual background of 4.7 ± 0.5 pb, mainly from the $\rm q\bar{q}(\gamma)$ final state.

5.1.2 The Semileptonic Channel

The selection of semileptonic candidates was optimized to keep events where the lepton is a muon or an electron. Events with tau-leptons in the final state were rejected because they contain less information about $m_{\rm W}$, due to neutrinos and because tau events require prior knowledge of $m_{\rm W}$ for use in a kinematic fit if they are to be efficiently selected from data.

The events were selected with the same criteria as for the cross-section measurement (sec. 4.2) except for the following:

- Both electrons and muons were required to be positively identified as described previously;
- The reconstructed lepton energies were required to be above 23 GeV;
- The isolation of the lepton candidate had to be at least 10°.

After the selection 11 electron and 12 muon candidates remained with W mass, reconstructed as described in the next section, between 73 and 85 GeV/c^2. The numbers of selected events expected from simulation are 10.3 with 1.0 background in the electron channel and 14.0 with 0.3 background in the muon channel.

The selections were made with different purpose than those used for the cross-section measurement (sec. 4). The fully hadronic selection was looser, since the background has little effect on the mass measurement and the increased efficiency reduces any possible bias. The semileptonic selection was more severe, since the distribution of masses from background with a lepton coming from the jet fragmentation is less under control.

5.2 Kinematic Reconstruction

The masses of the events were reconstructed using a constrained fitting algorithm. Each fitted element – lepton, jet or neutrino – was described by three parameters.

Muons were described by their measured momenta and their polar and azimuthal angles. The measurement errors were obtained directly from the track fit. Only the momentum error played any significant role for the precision of the m_{W} determination.

Electrons were characterized by their measured energies and their detected angular position in the electromagnetic calorimeters. The measurement errors were obtained from parametrizations of the responses of the electromagnetic calorimeters, which were tuned to the responses found in Bhabha and Compton scattering events. The angular errors were determined from the detector granularity and were significant only for the forward electromagnetic calorimeter.

The fitted jet momentum, $\vec{p_j}^{\,f}$, was projected onto a set of axes with one component parallel to the measured jet momentum, $\vec{p_j}^{\,m}$, and two transverse components. The parallel component was described by a rescaling factor, $\exp(a_j)$, while the transverse components were described by parameters multiplying perpendicular momenta fixed to 1 GeV/c:

$$\vec{p_j}^{\,f} = \exp(a_j)\vec{p_j}^{\,m} + b_j\vec{p_j}^{\,b} + c_j\vec{p_j}^{\,c}. \tag{3}$$

The directions of $\vec{p_j}^{\,b}$ and $\vec{p_j}^{\,c}$ were determined by a method described below.

The jet energy, ${E_j}^m$, and thereby also to a good approximation the jet mass, was rescaled with the same factor $\exp(a_j)$ as the jet momentum.

The fitting algorithm then minimized a χ^2:

$$\chi^2 = \sum_j \frac{(a_j - a_0)^2}{\sigma_{a_j}^2} + \frac{b_j^2}{\sigma_{b_j}^2} + \frac{c_j^2}{\sigma_{c_j}^2}, \tag{4}$$

while forcing the fitted event to obey the constraints.

The expected energy loss parameter, a_0, and the energy spread parameter, σ_{a_j}, were parametrized as functions of the angle of the jet with respect to the beam axis, $\cos\theta_j$. The transverse momentum errors depended on how broad the jets were. The broadness of a jet was calculated by projecting the momenta of all the particles belonging to the jet onto the plane perpendicular to the jet axis and forming a 2-dimensional momentum tensor $\mathcal{T}_{\beta\gamma}$:

$$\mathcal{T}_{\beta\gamma} = \sum_k p_\beta^k p_\gamma^k, \tag{5}$$

where p_β^k and p_γ^k are the two components of the projection of the momentum of particle k.

The normalized eigenvectors of the tensor, $\vec{p_j}^{\,b}$ and $\vec{p_j}^{\,c}$, then give the directions where the jet is broadest and slimmest. The corresponding eigenvalues are B_b and B_c. The transverse momentum errors also depended on how much energy remained undetected in the jet. This quantity, $E_{j\,\mathrm{miss}}$, was estimated for each jet by first performing a constrained fit for each event with transverse errors set to 1.5 GeV/c.

The momenta and directions of the primary quarks in simulated events can be used to estimate the experimental errors on the jet parameters. However, hard gluon radiation often induces distortions and ambiguities which reduce the performance of this procedure. Instead, the jet errors were tuned so that the analysis produced a pull distribution with a width within 1% of unity. The pull is defined as the reconstructed mass minus the nominal W mass divided by the error, and was evaluated for samples simulated with an integrated luminosity equal to the data.

Since the effects of overlapping jets are more severe in the fully hadronic channel than in the semileptonic channel, the tuned jet errors were different in the two cases. The following parametrizations were used:

For the fully hadronic events:

$$\begin{aligned}
a_0 &= 0.15 + 0.40 \cdot \cos^4\theta_j \\
\sigma_{a_j} &= 0.27 + 0.72 \cdot \cos^4\theta_j \\
{\sigma_{b_j}}^2 &= 0.36 + 1.8\,(\mathrm{GeV}/c)^{-2} \cdot B_b \frac{\sqrt{1\mathrm{GeV} \cdot {E_j}^m + E_{j\,\mathrm{miss}}^2}}{{E_j}^m} + 0.036\,(\mathrm{GeV}/c)^{-4} \cdot {B_b}^2 \\
{\sigma_{c_j}}^2 &= 0.36 + 1.8\,(\mathrm{GeV}/c)^{-2} \cdot B_c \frac{\sqrt{1\mathrm{GeV} \cdot {E_j}^m + E_{j\,\mathrm{miss}}^2}}{{E_j}^m} + 0.036\,(\mathrm{GeV}/c)^{-4} \cdot {B_c}^2 . \qquad (6)
\end{aligned}$$

For the semileptonic events:

$$\begin{aligned}
a_0 &= 0.15 + 0.40 \cdot \cos^6\theta_j \\
\sigma_{a_j} &= 0.15 + 0.40 \cdot \cos^6\theta_j \\
{\sigma_{b_j}}^2 &= 0.2 + 1.0\,(\mathrm{GeV}/c)^{-2} \cdot B_b \frac{\sqrt{1\mathrm{GeV} \cdot {E_j}^m + E_{j\,\mathrm{miss}}^2}}{{E_j}^m} \\
{\sigma_{c_j}}^2 &= 0.2 + 1.0\,(\mathrm{GeV}/c)^{-2} \cdot B_c \frac{\sqrt{1\mathrm{GeV} \cdot {E_j}^m + E_{j\,\mathrm{miss}}^2}}{{E_j}^m} . \qquad (7)
\end{aligned}$$

The neutrino momentum vector was considered as unknown, which led to a reduction of three in the number of constraints. The total χ^2 was then minimized by an iterative procedure using Lagrange multipliers for the constraints.

The value of m_{W} and its error were calculated from the fitted momenta. Events for which the χ^2 of the fit was larger than the number of degrees of freedom for the fit, NDF, had their errors scaled by a factor of $\sqrt{\chi^2/\mathrm{NDF}}$ in order to take non-Gaussian resolution effects into account.

The mass errors depend on the value of the computed masses, going to zero at the kinematic limit, which leads to asymmetric errors. In order to avoid any bias due to this effect, an additional 0.5 GeV/c^2 was added in quadrature to the mass error. This increased the widths of the likelihood curves (Section 5.3) by only 1% and changed the overall analysis bias (Section 5.3) by less than 0.01 GeV/c^2.

5.3 Calculation of the Likelihood for m_{W}

The resolution on the average of the two reconstructed W masses is found to be much better than that on the difference of the masses. This is due to the negative correlation between the two computed masses. Therefore only one mass was extracted per fit. In the constrained fit this was implemented as an additional equal mass constraint. The distributions of the reconstructed mass are shown in Fig. 6 for real and simulated data in the semileptonic and fully hadronic channels. For the fully hadronic channel only events with $D_{\mathrm{pur}} > 13$ GeV and only the combination with the lowest χ^2 are shown. The treatment of the different combinations in the fully hadronic events is described below.

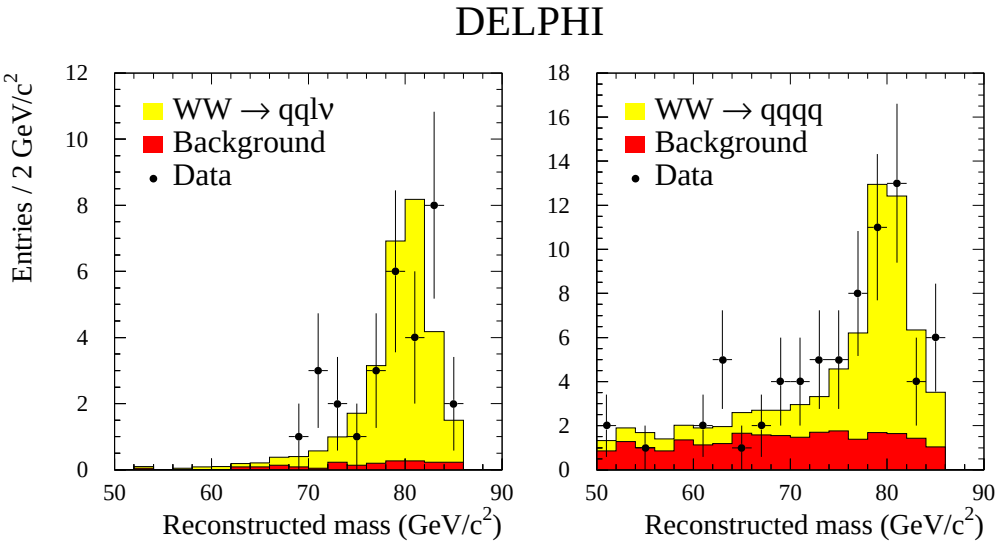

Figure 6: The distributions of the reconstructed masses for the semileptonic and fully hadronic channels.

The information on the W mass was then extracted from the likelihood of observing each individual event.

In the case of semileptonic candidates the likelihood is expressed as

$$\mathcal{L}(m_{\mathrm{W}}) = P\left(\int_0^{E_b} \mathrm{G}(m_{\mathrm{f}}|m)\cdot \mathrm{BW}(m|m_{\mathrm{W}})\cdot \mathrm{PS}(m)dm\right) + (1-P)p_{\mathrm{b}}(m_{\mathrm{f}}), \qquad (8)$$

where P is the overall fraction of events expected from simulation to be signal (90% for the electron events and 98% for the muon events); E_b is the beam energy; $\mathrm{G}(m_{\mathrm{f}}|m)$ is a Gaussian resolution function

$$\mathrm{G}(m_{\mathrm{f}}|m) = \frac{1}{\sqrt{2\pi}\sigma_{\mathrm{f}}}\exp\left(-\frac{(m_{\mathrm{f}}-m)^2}{2\sigma_{\mathrm{f}}^2}\right), \qquad (9)$$

where m_{f} is the value of the fitted mass and σ_{f} is the error on m_{f}; $\mathrm{BW}(m|m_{\mathrm{W}})\cdot\mathrm{PS}(m)$ is the expected distribution of the average of two W masses

$$\mathrm{BW}(m|m_{\mathrm{W}})\cdot\mathrm{PS}(m) \propto \frac{\Gamma_{\mathrm{W}}}{m_{\mathrm{W}}}\frac{m^2}{(m^2-m_{\mathrm{W}}^2)^2 + m^4\Gamma_{\mathrm{W}}^2/m_{\mathrm{W}}^2}\sqrt{E_b^2-m^2}, \qquad (10)$$

where the width of the W resonance is taken as $\Gamma_{\mathrm{W}} = 2.07$ GeV/c^2; and the shape of the background distribution, $p_{\mathrm{b}}(m_{\mathrm{f}})$, was taken numerically from simulation. Only

events with a reconstructed mass between 73 GeV/c^2 and 85 GeV/c^2 were used in the semileptonic analysis in order to reject possible non-resonant background events. The production probability, $\mathrm{BW}(m|m_\mathrm{W}) \cdot \mathrm{PS}(m)$, in eq. (10) was normalized to unity.

The treatment of the fully hadronic candidates was more involved due to multiple combinations. In the case of 4-jet events there are three ways of choosing a di-jet combination, while 5-jet events led to 10 possible combinations. However, the measured mass difference can be used to differentiate between the combinations. The fully hadronic candidates were therefore fitted without the equal mass constraint, leading to a mass difference Δ_i with an error $\sigma_{\Delta i}$ for each possible combination, i. The distribution of the mass difference for the correct combination is a convolution of the experimental resolution and the difference coming from the relativistic Breit-Wigner distributions:

$$p_i(\Delta_i) \propto \int_{-\infty}^{\infty} \frac{1}{\Delta^2 + {\Gamma_\mathrm{W}}^2} \exp\left(-\frac{(\Delta_i - \Delta)^2}{2{\sigma_{\Delta_i}}^2}\right) d\Delta. \tag{11}$$

The distribution due to wrong combinations can be assumed to be uniform close to $\Delta = 0$, so that the relative probabilities of the combinations can be estimated as the ratios of the p_i. For the 5-jet candidates the relative probability to have gluon radiation was estimated as:

$$p_i^g(k_\perp^g) dk_\perp^g \propto \frac{\alpha_\mathrm{s}(k_\perp^g)}{k_\perp^g} dk_\perp^g, \tag{12}$$

where $k_\perp^g$, the transverse momentum of the gluon relative to the quark-antiquark pair which radiated the gluon, was estimated as the minimum $k_\perp$ of the three possible gluon candidates. Each of the ten probabilities was therefore multiplied by $\frac{1}{k_\perp^g}$ and the sum of the probabilities normalized to unity.

In the fully hadronic final state there is a further complication arising from the fact that the jet reconstruction procedure does not always perform a fully correct clustering. The efficiency, ϵ_c, for a jet reconstruction without major faults was estimated from simulation to be 85% for 4-jet and 75% for 5-jet events. The value of ϵ_c is correlated with the measurement errors described above. The likelihood for observing a fully hadronic candidate is a sum over all the possible combinations:

$$\begin{aligned}\mathcal{L}(m_\mathrm{W}) = \sum_i p_i \cdot \Bigg(P(D_\mathrm{pur}) \quad & \Bigg[\quad \epsilon_\mathrm{c} \Bigg(\int_0^{E_b} \mathrm{G}(m|m_\mathrm{i}) \cdot \mathrm{BW}(m|m_\mathrm{W}) \cdot \mathrm{PS}(m) dm \Bigg) \\ & + \quad (1 - \epsilon_\mathrm{c}) p_\mathrm{c}(m_\mathrm{i}) \Bigg] + (1 - P(D_\mathrm{pur})) p_\mathrm{b}(m_\mathrm{i}) \Bigg),\end{aligned} \tag{13}$$

where $p_\mathrm{c}(m_\mathrm{i})$ (the distribution of the wrong combinations) and $p_\mathrm{b}(m_\mathrm{i})$ were extracted from simulation, and $P(D_\mathrm{pur})$ is the event purity described in Section 5.1.1.

Since the candidate events are not correlated, the combined likelihood for observing all the events is the product of all the event likelihoods. Equivalently, a $\Delta\chi^2$ value was extracted as:

$$\Delta\chi^2(m_\mathrm{W}) = \sum_k -2 \ln \mathcal{L}_k(m_\mathrm{W}) - \sum_k -2 \ln \mathcal{L}_k(m_{\mathrm{W\,max}}), \tag{14}$$

where $m_{\mathrm{W\,max}}$ is the value of m_W for which the likelihood is largest and the sum is taken over all accepted events. The final likelihood curves are shown in Figs. 7 and 8.

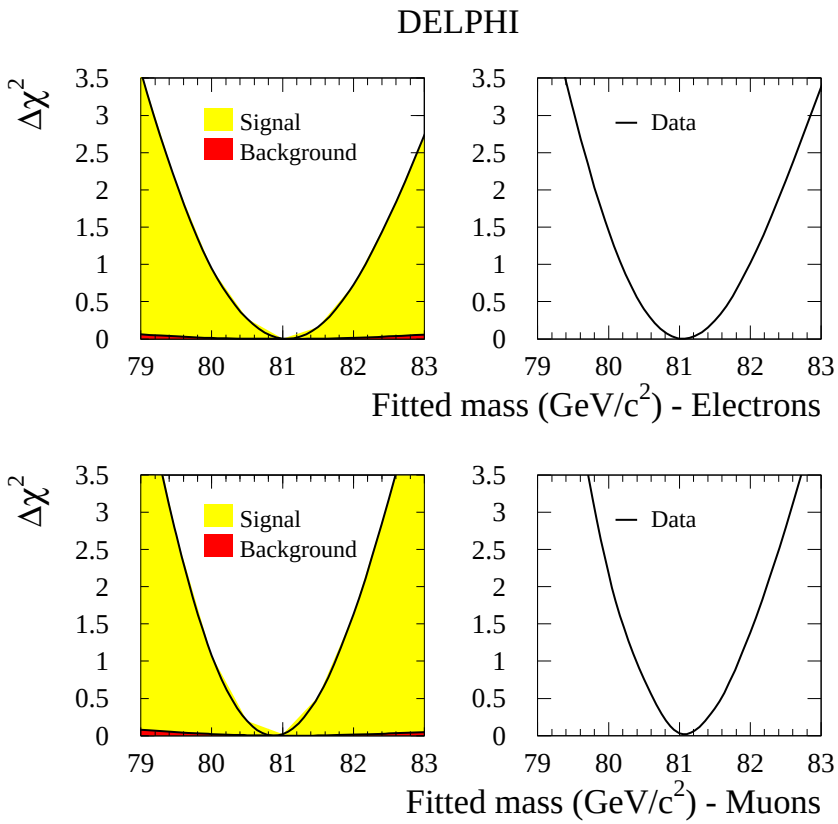

Figure 7: The likelihood curves for the semileptonic analysis. The plots on the right show the likelihood curves resulting from the analysis of the real data while those on the left show the average expected likelihood curves from events simulated with $m_{\mathrm{W}} = 80.35$ GeV/c^2.

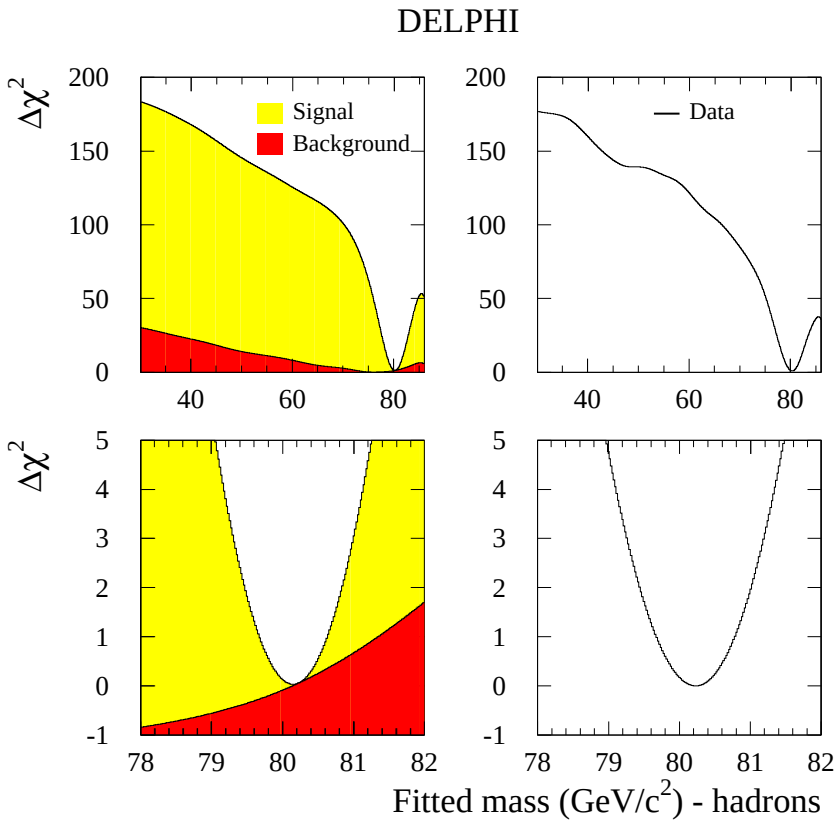

Figure 8: The likelihood curves for the fully hadronic analysis. The plots on the right show the likelihood curve resulting from the analysis of the real data while those on the left show the average expected likelihood curve from events simulated with $m_{\mathrm{W}} = 79.85$ GeV/c^2. The lower plots show the region around the fitted value of m_{W} in more detail.

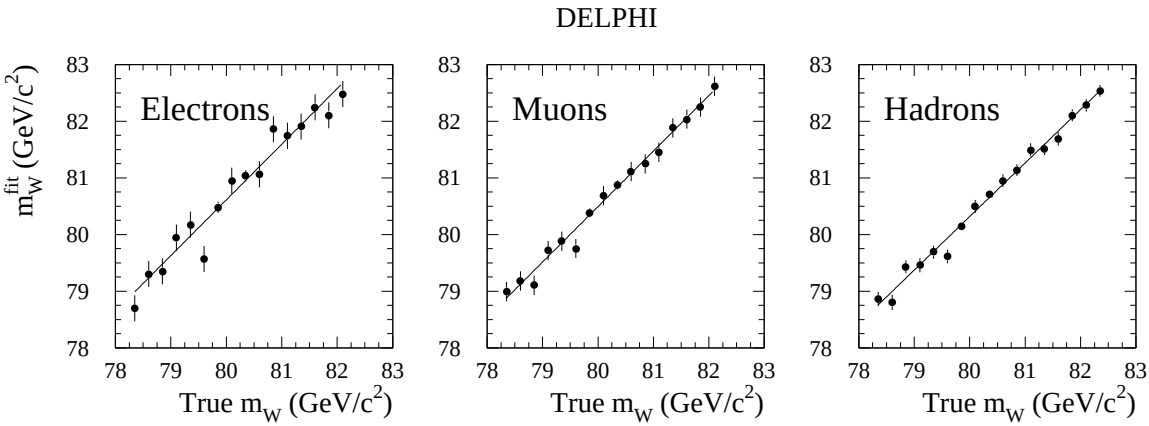

Figure 9: Fitted versus generated W mass for $q\bar{q}e\nu$, $q\bar{q}\mu\nu$ and $q\bar{q}q\bar{q}$ events together with linear fits.

The fitted value of m_W is biased because not all detector and physics effects are taken into account in the likelihood description. In order to correct for this bias a calibration procedure was performed using simulated event samples generated with different values of m_W. The analysis response as a function of m_W is shown in Fig. 9. It is consistent with being linear over the mass range considered and a fit to the expression:

$$m_{\rm rec} - m_{\rm ref} = a(m_{\rm gen} - m_{\rm ref}) + b \tag{15}$$

was used to extract the correction, where $m_{\rm ref}$ is the value of the generated mass for which the result of the analysis of simulated events is closest to that of the data, and was found to be 80.35 and 79.85 GeV/c^2 for the semileptonic and fully hadronic channels respectively.

The scale factor, a, is slightly below unity, which is expected from the effect of initial state radiation. The bias, b, is positive and dominated by initial state radiation and the measurement errors being negatively correlated with the fitted mass. The latter effect leads to an asymmetric experimental response function which has not been taken into account in the likelihood expression. The statistical errors on m_W were checked by performing a large set of simulated experiments and verifying that the observed variance corresponds to the expected one within a precision of 1%. The statistical errors were corrected using the same scale factor as was applied to the fitted m_W. The final measured values are shown in Table 3.

Numerically large statistical fluctuations can be expected in data samples with low statistics. Figure 10 shows the distribution of errors on m_W from samples of simulated fully hadronic events with an integrated luminosity of 9.98 pb^{-1}. Figure 10 also shows the width of the pull distribution as a function of the likelihood error. It is nearly independent of the error, signifying that the likelihood error can be relied upon.

	Electrons	Muons	Hadrons
Expected error on m_W (GeV/c^2)	1.09	0.76	0.52
a	0.97 ± 0.05	0.98 ± 0.04	0.94 ± 0.02
b (GeV/c^2)	0.60 ± 0.05	0.48 ± 0.04	0.33 ± 0.02
Fitted mass on data sample (GeV/c^2)	81.05 ± 0.85	81.04 ± 0.72	80.23 ± 0.56
Measured W mass (GeV/c^2)	**80.45±0.87**	**80.56±0.76**	**79.90±0.59**

Table 3: Results of the analysis of the $q\bar{q}e\nu$, $q\bar{q}\mu\nu$ and $q\bar{q}q\bar{q}$ channels. The expected error is after calibration. a is the scale factor from the calibration procedure and b is the bias from analysis. The measured value of m_W is given before and after the calibration correction.

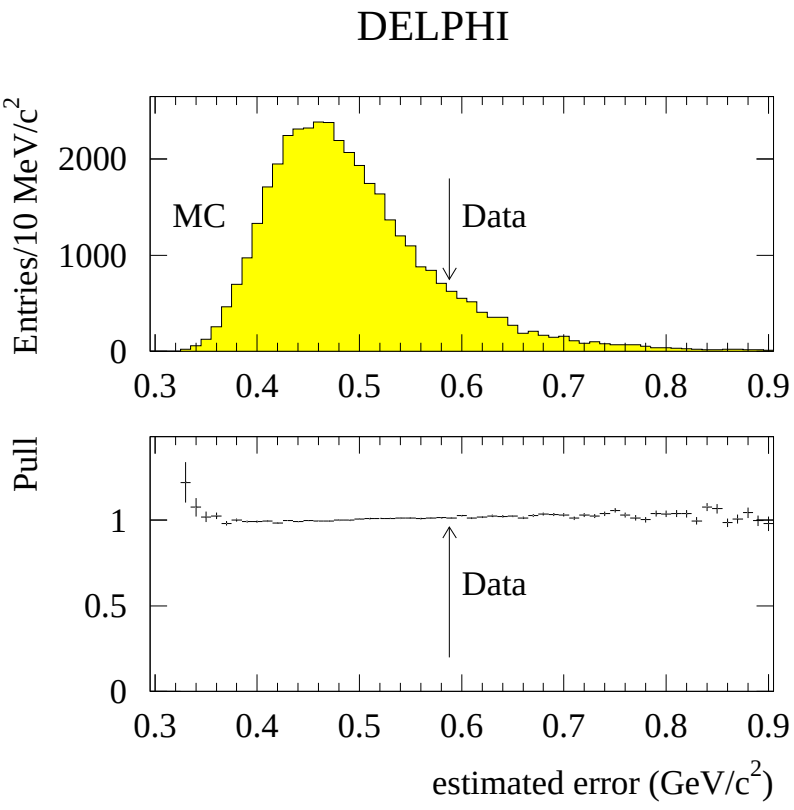

Figure 10: The distribution of errors on m_W from samples of simulated hadronic events. The upper plot shows the distribution. The lower plot shows the width of the pull distribution as a function of the error on m_W. The arrow indicates the value of the likelihood error from the data.

5.4 Systematic Errors

The analysis described above is largely model independent, but does rely on corrections obtained from simulation. Any error in the simulation will cause a wrong bias and thereby a systematic error.

The systematic uncertainty on the beam energy is slightly above 30 MeV [13] which corresponds to a systematic error on m_W of 30 MeV/c^2.

The uncertainties on the correction for the bias are 50, 40, and 25 MeV/c^2 for the electron, muon and fully hadronic channels. These errors come from limited simulation statistics and are uncorrelated between channels.

The possible systematic error from the description of the response of the DELPHI detector to hadronic jets has been evaluated using the Z^0 data collected during the 1996 data taking. Discrepancies between the reconstructed jet energies in real and simulated hadronic Z^0 decays were evaluated and parametrized as a function of the polar angle. The simulated events were then corrected to remove these discrepancies, both by rescaling the measured energies and by throwing particles away at random. This led to changes in the bias of up to 30 MeV/c^2, which has been used as a systematic error. This error was taken to be fully correlated for the electrons and muons, while only half of it was taken to be correlated between the semileptonic and fully hadronic channels because of the different impact of the jet energy measurement after the constrained fit.

The systematic uncertainty on the muon momentum was estimated from $Z^0 \to \mu^+\mu^-$ events to be 0.5%, while the Bhabha and Compton scattering events showed an uncertainty on the electron energy of 1%. This corresponds to uncorrelated systematic errors of 10 and 15 MeV/c^2 respectively.

The impact of an incorrect description of the jet fragmentation led to an estimated fully correlated systematic error on m_{W} in the semileptonic channels of 10 MeV/c^2 due to limited simulation statistics. For the fully hadronic channels the situation is less clear due to the overlap of jets from different W decays. This error was studied by looking at the difference between two simulated samples generated with JETSET [6] and ARIADNE [14], which have different treatments of the parton shower, used in conjunction with a simplified simulation of the DELPHI detector. A difference in m_{W} of 2 ± 25 MeV/c^2 was found, where the statistical error was taken as the systematic error contribution.

The impact of the background on the semileptonic channel was very small and a change of $\pm10\%$ led to correlated changes of 5 MeV/c^2 in the bias, which was taken as the systematic error. The background plays a more important part in the fully hadronic analysis, but the inclusion of event-by-event purity values reduced its impact. Completely omitting the background changed the bias by 90 MeV/c^2. Thus the systematic error on the level of background left a systematic uncertainty of 10 MeV/c^2, while the difference between the JETSET and ARIADNE Monte Carlo generators was used to estimate an uncertainty of 10 MeV/c^2 coming from the shape of the background mass distribution.

The effects of the interference between the CC03 diagrams and the additional diagrams as described in the cross-section measurement were estimated at generator level. Except for the electron channel the effect was found to be small and a systematic error of 10 MeV/c^2 was estimated. The electron channel is more affected due to the interference with the single W production, leading to a positive shift of 50 MeV/c^2 at the generator level when the mass was estimated from a lineshape fit. A simplified detector study on this channel gave compatible results. The fitted value of m_{W} was corrected for this effect in the electron channel and a systematic error of 50 MeV/c^2 was assigned.

The systematic error coming from the uncertainty of the simulation of initial state radiation was assigned to be 10 MeV/c^2 [8], fully correlated between the channels.

5.4.1 Interconnection Effects

At the collision energies which can be reached at LEP2, the W bosons are typically separated by $\mathcal{O}(0.1$ fm) when they decay. This is much smaller than the typical hadronisation scale, and interactions between the two systems can therefore influence the W mass distribution in the case where both W bosons decay hadronically. Two potentially

Channel Source of systematic error	Electrons	Muons	Semi- leptonic	Fully hadronic	All Combined
Beam energy	30	30	30	30	30
Calibration of analysis bias	50	40	31	25	20
Detector response to jets	30	30	30	30	26
Lepton energy	15	10	9	0	5
Jet Fragmentation	10	10	10	25	13
Level of background	5	5	5	10	6
Shape of background	0	0	0	10	5
4-fermion correction	50	10	22	10	12
ISR	10	10	10	10	10
Colour reconnection	0	0	0	100	48
Bose-Einstein	0	0	0	20	10
Total error (MeV/c^2)	**85**	**62**	**60**	**116**	**70**

Table 4: A breakdown of the systematic errors from the direct reconstruction of m_{W}.

significant effects have been identified: Colour reconnection in the non-perturbative stage of hadronisation [15,16], and Bose-Einstein correlations among identical bosons from the two W bosons [17].

In the case of colour reconnection, several phenomenological studies have been performed [16,18–21], but the results are inconclusive. We therefore decided to assign a nominal systematic error of 100 MeV/c^2 from this source [22]. A study claiming the possibility of a substantially larger effect [23] also predicts a substantial decrease in the multiplicity [24], which is disfavoured by the data [25].

For Bose-Einstein correlations, the first study [17] indicated possible effects on the W mass of the order of 100 MeV/c^2, but more recent studies [26,27] give much smaller effects, in part due to the realization that the value of the mass determined from a fit to the lineshape is much less sensitive to the effect than the average mass considered in [17]. Furthermore, the first measurement of Bose-Einstein correlations in WW events has shown no evidence for such correlations between pions from different W bosons [28]. A nominal systematic error of 20 MeV/c^2 was therefore assigned to this effect.

All the systematic errors for each of the channels and for combinations of channels are shown in Table 4.

6 Combined Measurement of m_{W}

Combining the results from the two semileptonic decay channels yields:

$$m_{\mathrm{W}} = 80.51 \pm 0.57(\mathrm{stat.}) \pm 0.05(\mathrm{syst.}) \pm 0.03(\mathrm{LEP})\ \mathrm{GeV}/c^2.$$

Combining the results from the semileptonic and hadronic decays yields:

$$m_{\mathrm{W}} = 80.22 \pm 0.41(\mathrm{stat.}) \pm 0.04(\mathrm{syst.}) \pm 0.05(\mathrm{int.}) \pm 0.03(\mathrm{LEP})\ \mathrm{GeV}/c^2,$$

where "int." stands for the uncertainty due to interconnection.

The cross-section for $\mathrm{e^+e^-} \to \mathrm{W^+W^-}$ near threshold is also sensitive to the value of m_{W} and was used to derive a value for m_{W} from 161 GeV data [1], assuming the validity of the cross-section dependence predicted by the Standard Model. The same procedure was applied to the 172 GeV data, using the cross-section derived in Section 4.4, though

the sensitivity to m_{W} is reduced at this higher energy. The combined value of m_{W}, using cross-section measurements at both energies, was determined to be:

$$m_{\mathrm{W}} = 80.45 \pm 0.43(\mathrm{stat.}) \pm 0.09(\mathrm{syst.}) \pm 0.03(\mathrm{LEP})\ \mathrm{GeV}/c^2.$$

Combining the W mass obtained from the cross-section measurement with the direct reconstruction result yields:

$$m_{\mathrm{W}} = 80.33 \pm 0.30(\mathrm{stat.}) \pm 0.05(\mathrm{syst.}) \pm 0.03(\mathrm{int.}) \pm 0.03(\mathrm{LEP})\ \mathrm{GeV}/c^2.$$

7 Summary

From a data sample of 9.98 pb^{-1} integrated luminosity, collected by DELPHI in $\mathrm{e^+e^-}$collisions at a centre-of-mass energy of 172 GeV, the W hadronic branching fraction was measured to be

$$\mathrm{Br(W} \to \mathrm{q\bar{q}}) = 0.660^{+0.036}_{-0.037}(\mathrm{stat.}) \pm 0.009(\mathrm{syst.})$$

and the cross-section for the doubly resonant process was measured to be $\mathrm{e^+e^-} \to \mathrm{W^+W^-} = 11.58^{+1.44}_{-1.35}(\mathrm{stat.}) \pm 0.32(\mathrm{syst.})$ pb assuming Standard Model branching fractions.

The mass of the W boson has been obtained from direct reconstruction of the invariant mass of the fermion pairs in the decays $\mathrm{WW} \to \ell\nu\mathrm{q\bar{q}}$ and $\mathrm{WW} \to \mathrm{q\bar{q}q\bar{q}}$ and found to be

$$m_{\mathrm{W}} = 80.22 \pm 0.41(\mathrm{stat.}) \pm 0.04(\mathrm{syst.}) \pm 0.05(\mathrm{int.}) \pm 0.03(\mathrm{LEP})\ \mathrm{GeV}/c^2.$$

Combined with the W mass obtained from the cross-sections measured by DELPHI, a value of

$$m_{\mathrm{W}} = 80.33 \pm 0.30(\mathrm{stat.}) \pm 0.05(\mathrm{syst.}) \pm 0.03(\mathrm{int.}) \pm 0.03(\mathrm{LEP})\ \mathrm{GeV}/c^2$$

was found.

These results are compatible with those found by the other LEP collaborations [29].

Acknowledgements

We thank the SL division of CERN for the excellent performance of the LEP collider and their careful work on the beam energy determination. We are also grateful to the technical and engineering staffs in our laboratories and to our funding agencies for their continuing support.

References

[1] DELPHI Collaboration: P. Abreu et al., Phys. Lett. **B397** (1997) 158.
[2] DELPHI Collaboration: P. Aarnio et al., Nucl. Instr. & Meth. **A303** (1991) 233.
[3] DELPHI Collaboration: P. Abreu et al., Nucl. Instr. & Meth. **A378** (1996) 57.
[4] A. C. Benvenuti et al., *The DELPHI Small Angle Tile Calorimeter*, contribution to IEEE NSS 1994, IEEE Trans. Nucl. Sci. **42** (4) (1995) 478.
[5] S. Jadach, O. Nicrosini et al., *Event Generators for Bhabha Scattering*, Physics at LEP2, eds. G.Altarelli, T.Sjöstrand and F.Zwirner, CERN 96-01 (1996) Vol 2, 229.
[6] T. Sjöstrand, *PYTHIA 5.719 / JETSET 7.4*, Physics at LEP2, eds. G. Altarelli, T. Sjöstrand and F. Zwirner, CERN 96-01 (1996) Vol 2, 41.
[7] DELPHI Collaboration: P. Abreu et al., Z. Phys. **C73** (1996) 11.
[8] W. Beenakker, F. A. Berends et al., *WW Cross-Section and Distributions*, Physics at LEP2, eds. G. Altarelli, T. Sjöstrand and F. Zwirner, CERN 96-01 (1996) Vol 1, 79.
[9] T. Sjöstrand, *PYTHIA 5.7 / JETSET 7.4*, CERN-TH.7112/93 (1993).
[10] P. Abreu, D. Fassouliotis, A. Grefrath, R.P. Henriques and L. Vitale, *SPRIME, A Package for Estimating the Effective* $\sqrt{s'}$ *Centre of Mass Energy in* $q\bar{q}(\gamma)$ *Events*, internal DELPHI note 96-124 PHYS 632 (1996), unpublished.
[11] D. Bardin, M. Bilenky, D. Lehner, A.Leike, A. Olshevski and T. Riemann, DESY 95-167 (1995).
[12] S. Catani et al., Phys. Lett. **B269** (1991) 432;
N. Brown and W. J. Stirling, Z. Phys. **C53** (1992) 629.
[13] The working group for LEP energy, *LEP Energy Calibration in 1996*, LEP Energy Group/97-01 (1997), unpublished.
[14] L. Lönnblad, Comp. Phys. Comm. **71** (1992) 15.
[15] G. Gustafson et al., Phys. Lett. **B209** (1988) 90.
[16] T. Sjöstrand and V. Khoze, Phys. Rev. Lett. **72** (1994) 28;
T. Sjöstrand and V. Khoze, Z. Phys. **C62** (1994) 281.
[17] L. Lönnblad and T. Sjöstrand, Phys. Lett. **B351** (1995) 293.
[18] G. Gustafson and H. Häkkinen, Z. Phys. **C64** (1994) 659.
[19] B. Webber, *QCD event generators*, Physics at LEP2, eds. G. Altarelli, T. Sjöstrand and F. Zwirner, CERN 96-01 (1996) Vol 2, 161–162.
[20] L. Lönnblad, CERN-TH/95-218 (1995).
[21] S. Todorova, *QCD event generators*, Physics at LEP2, eds. G. Altarelli, T. Sjöstrand and F. Zwirner, CERN 96-01 (1996) Vol 2, 159–160.
[22] Z. Kunszt, W. J. Stirling et al., *Determination of the mass of the W boson*, Physics at LEP2, eds. G. Altarelli, T. Sjöstrand and F. Zwirner, CERN 96-01 (1996) Vol 1, 141–205.
[23] J. Ellis and K. Geiger, Phys. Rev. **D54** (1996) 1967.
[24] J. Ellis and K. Geiger, Phys. Lett. **B404** (1997) 230.
[25] DELPHI Collaboration: P. Abreu et al., *Charged Particle Multiplicity in* $e^+e^- \to q\bar{q}$ *events at 161 and 172 GeV and from the Decay of the W Boson*, CERN-PPE/97-113, to be published in Phys. Lett. B.
[26] V Kartvelishvili, R. Kvatadze and R. Møller, Phys. Lett. **B408** (1997) 331.
[27] S. Jadach and K. Zalewski, Acta Phys. Polonica, **B28** (1997) 1363.
[28] DELPHI Collaboration: P. Abreu et al., Phys. Lett. **B401** (1997) 181.
[29] Aleph Collaboration: *Measurement of the W-pair cross section in* e^+e^- *collisions at 172 GeV*, CERN PPE/97-102, submitted to Phys. Lett B;

L3 Collaboration: M. Acciarri et al., *Measurements of Mass, Width and Gauge Couplings of the W Boson at LEP*, CERN-PPE/97-98, to appear in Phys. Lett. B;
OPAL Collaboration: K. Ackerstaff et al., *Measurement of the W Boson Mass and W^+W^- Production and Decay Properties in e^+e^- Collisions at $\sqrt{s}$ = 172 GeV*, CERN-PPE/97-116, submitted to Z. Phys. C.